Catena 267 (2026) 109963

Contents lists available at ScienceDirect

Catena

journal homepage: www.elsevier.com/locate/catena

A century-scale sedimentary organic matter record of the South Yellow Sea: Response to climatic and anthropogenic changes in the Yellow River Basin

Chuchu Zhang [a,b], Yifei Qiu [b], Xiao Huang [b], Xinqing Zou [b,c], Min Xu [a,*], Chenglong Wang [b,*]

[a] School of Marine Science and Engineering, Nanjing Normal University, Nanjing 210023, China
[b] School of Geography and Ocean Science, Ministry of Education Key Laboratory for Coast and Island Development, Nanjing University, Nanjing 210093, China
[c] Collaborative Innovation Center of South China Sea Studies, Nanjing University, Nanjing 210093, China

ARTICLE INFO

Keywords:
South yellow sea
Yellow river basin
Terrestrial organic matter
Climate change
Human activities

ABSTRACT

The burial of organic carbon (OC) in marine sediments plays a critical role in the global carbon cycle, with marginal seas being particularly important. The Yellow Sea possesses one of the most extensive continental shelves globally, which receives vast amounts of sediment from the Yellow River. To investigate the fate of sedimentary organic matter (OM) and the response of OM fate to climatic and anthropogenic changes in the Yellow River Basin over the past two centuries, a sediment core H28 from the South Yellow Sea Central mud deposit was analyzed using lignin phenols and bulk OM parameters. Rising temperatures with reduced precipitation have led to a decrease in the Yellow River's natural runoff, and has consequently diminished sediment transport in the river channel, which has finally contributed to a persistent decline in terrestrial OM (TOM) input since approximately 1970. Cultivation and deforestation, which driven by rapid population growth, have led to a reduction in forest cover, an increase in soil erosion, and eventually an elevated input of TOM before 1970. Simultaneously, human activities such as dam construction, soil conservation measures, and increased water consumption have significantly reduced sediment load from the Yellow River, further decreasing the supply of TOM since around 1970. Unlike the declining trends in both eight major lignin phenols (Σ8) content and TOM contribution observed around 1970, total OC (TOC) and total nitrogen (TN) content consistently maintained an increasing trend due to severe eutrophication and the increasing contribution of marine organic matter. Notably, despite a sharp decrease in mass accumulation rate since 1970, OC accumulation rate has exhibited a gradual increasing trend.

1. Introduction

The burial of organic carbon (OC) in marine sediments serves as the second largest long-term sink for atmospheric CO_2 and plays a critical role in the global carbon cycle, with marginal seas being particularly important (Berner, 1990; Burdige, 2005). Continental margins account for over 80% of this marine OC burial (Berner, 1982; Burdige, 2007), where sedimentary organic matter (OM) constitutes a complex mixture of terrestrial and marine sources (Blair and Aller, 2012). Clarifying the distribution and sources of sedimentary OM in marginal seas helps reveal the mechanisms of dispersal, preservation, and fate of OM at continental margins (Gordon and Goñi, 2003; Tesi et al., 2007), which is of great significance for deepening our understanding of the global carbon cycle (Hedges et al., 1997).

Over the past century, sedimentary records have captured clear signals of dramatic changes, driven by both climatic shifts and human activities. These include shifts in terrestrial OM (TOM) inputs, fluctuations in primary productivity, and intensified anthropogenic disturbances, all of which have profoundly influenced the fate and dynamics of sedimentary OM (Liu et al., 2013; Wang et al., 2021). Therefore, centennial-scale sedimentary records provide a crucial perspective for understanding the evolution of the modern marine carbon sink and its driving mechanisms, holding substantial scientific and practical value.

The eastern China marginal seas (Bohai Sea, Yellow Sea, and East China Sea) represent one of the largest continental margins globally, accounting for approximately 10% of OC stored in global ocean margins (Deng et al., 2006; Hu et al., 2016). These regions are characterized by significant spatial and temporal variability in physicochemical and biological conditions (Guo et al., 2021). This substantial contribution is primarily attributed to the massive supply of terrestrial materials from

* Corresponding authors.
E-mail addresses: xumin0895@njnu.edu.cn (M. Xu), clwang@nju.edu.cn (C. Wang).

https://doi.org/10.1016/j.catena.2026.109963
Received 30 September 2025; Received in revised form 2 February 2026; Accepted 26 February 2026

large river systems, notably the Yellow River and the Changjiang River (Deng et al., 2006; Hu et al., 2016; Zhao et al., 2021; Shi et al., 2024). Among them, the Yellow Sea, which receives vast amounts of sediment from the Yellow River, possesses one of the most extensive continental shelves globally (Park and Khim, 1990). South Yellow Sea Central mud deposit located in the central South Yellow Sea, are ideal for the study of long-term OM burial (Fig. 1), which is significant to the study of impact of centennial climate change and human activities on the fate of OM. Historically, the Yellow River is regarded as the second largest river of the world in terms of sediment load over the last several thousand years, with annual sediment load of 1.08 Gt/yr (Milliman and Meade, 1983; Wang et al., 2007). However, under the combined influence of global climate change and human activities, its river runoff and sediment load have declined significantly in recent decades. This pronounced reduction in terrestrial input has exerted profound influences on estuary-delta systems and adjacent seas, driving a cascade of responses, including shifts in sedimentary environments, reshaping of geomorphological features, ecosystem evolution, and disruptions to biogeochemical cycles (Deng and Jin, 2000; Wang et al., 2006a; Wang et al., 2020; Wang et al., 2025). Therefore, investigating the impacts of climate change and human activities within the Yellow River basin on the long-term transport and transformation processes of sedimentary OM in the South Yellow Sea is of great scientific significance for advancing our understanding of coastal carbon cycling under global change.

To investigate the variations in the deposition of sedimentary OM influenced by climate change and human activities, it is necessary to employ multiple proxy indicators to differentiate between TOM and marine OM (MOM) in sediments (Sikes et al., 2009). Elemental signatures, such as the C/N ratio and stable carbon isotope ratio ($\delta^{13}C$), can reveal the relative contributions of TOM and MOM (Meyers, 1997). However, employing these bulk parameters to investigate the sources of OM carries inherent uncertainties. In contrast, molecular biomarkers (such as n-alkanes, sterols, long-chain fatty acids, GDGTs, and lignin) represent potentially effective indicators for tracing OM sources and fates (Sikes et al., 2009; Zhao et al., 2021). Among these, lignin holds particular significance as the sole terrestrial biomarker produced by vascular plants, owing to its relative resistance to degradation and near-absence in MOM (Wang et al., 2015). Lignin acts as a tracer for investigating the transport of TOM from river basins to continental shelves and into deep-sea environments (Kuzyk et al., 2008).

In this study, lignin phenols and bulk OM properties were analyzed to describe the source, degradation, and burial of OM in the South Yellow Sea on a centennial scale. Parameters related to climate change (e.g., the intensity of the East Asian summer monsoon (EASM), East Asian winter monsoon (EAWM), precipitation and temperature) and human activities (including population, dam construction, soil and water conservation measures, water consumption and eutrophication) in the Yellow River basin were used to determine the key factors affecting the fate of OM in the past two centuries. Meanwhile, mass accumulation rate and OC accumulation rate were calculated to assess the capacity of the South Yellow Sea as a sink for sedimentary OC.

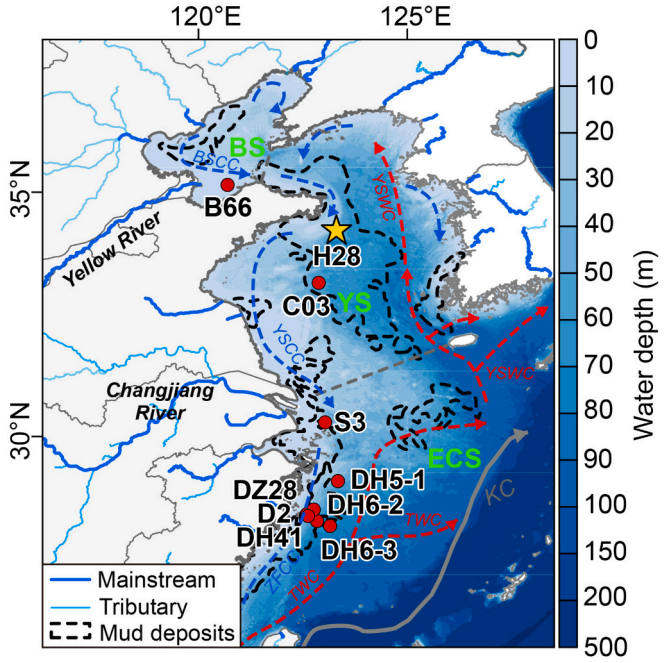

Fig. 1. Map showing the study area, location of core H28 (yellow pentagram) and other collected cores (B66, C03, S3, DH5–1, DH6–2, DH6–3, DZ28, D2, DH41) in the eastern China marginal seas (red dot) for reference. The sedimentation rates of core B66, C03, S3, DH5–1, DH6–2, DH6–3, DZ28, D2, DH41 was 0.48, 0.35, 2.44, 0.26, 0.39, 0.28, 0.89, 1.05, and 0.96 cm/yr. The sea area is shown in gradated shades of blue, with darker tones corresponding to greater water depth. Mud deposits in the eastern China marginal seas are shown within the black dotted line. BSCC: Bohai Sea Coastal Current, YSCC: Yellow Sea Coastal Current, YSWC: Yellow Sea Warm Current, ZFCC: Zhejiang-Fujian Coastal Current, KC: Kuroshio Current, TWC: Taiwan Warm Current. (For interpretation of the references to colour in this figure legend, the reader is referred to the web version of this article.)

2. Material and methods

2.1. Material

The South Yellow Sea is a typical river-dominated ocean margin, and receives large amounts of sediments from the Yellow River (Park and Khim, 1990). The modern circulation system includes the Yellow Sea Warm Current (YSWC), the Yellow Sea Coastal Current (YSCC), and the Korean Coastal Current (KCC) (Fig. 1; Yuan et al., 2008; Moon et al., 2009). The sediment core H28 (123.00°N, 36.50°E) was collected from the edge of South Yellow Sea Central mud deposits (Fig. 1) in August 2023, 62 km far from the coast. The water depth of H28 is 60.9 m and the length of core is 70 cm. The core was subsampled at 1 cm intervals to yield 70 sediment samples and stored at −20 °C.

2.2. Methods

2.2.1. Core lithology and chronology

To establish a robust chronological framework and calculate sedimentation rates, this study utilizes the radiometric dating method based on ^{210}Pb. With a half-life of approximately 22.3 years, ^{210}Pb is particularly effective for dating modern sediments and is an essential tool for reconstructing recent marine depositional processes and histories of environmental change. The pretreatment and testing of ^{210}Pb in the samples were completed at the Key Laboratory of Coastal and Island Development of the Ministry of Education, Nanjing University. First, the core sediment samples were ground to 100 mesh, and approximately 2 g of each sample was weighed and placed in a pretreatment container. We sequentially added deionized water, n-octanol, and a ^{209}Po tracer, then stepwise added 6 mL of concentrated HNO_3 and HF to dissolve the silicate matrix and organic matter, thus ensuring the complete release of the target radionuclides. After thorough shaking and mixing, the mixture was heated until completely evaporated. Then, 20 mL HCL was added and heated until the solution reached a viscous semi-dry state. This acid treatment step was repeated 4 times to ensure complete digestion for the removal of fluoride interference. Finally, 40 mL dilute HCL was added, and after centrifugation, the supernatant was collected and continuously heated on a constant-temperature electric stirrer for 5 h. The processed nickel sheets were rinsed multiple times with deionized water and air-dried at room temperature for later use. The samples were measured using a low-background alpha spectrometer (EG&G, USA).

The Constant Initial Concentration model (Goldberg and Koide, 1963) was applied to establish the chronological sequence of the

sediment core. The sediment accumulation rate R was calculated according to the formula:

$$R = \frac{H\lambda}{ln\frac{I_0}{I_h}} \quad (1)$$

where R is the sediment accumulation rate (cm/yr); H is the depth; λ is the decay constant of ^{210}Pb (0.03114 yr^{-1}); I_o is the ^{210}Pb activity at the surface of the sediment core; I_h is the ^{210}Pb activity at depth H. Using the sampling year 2023 as the dating reference point, the ages of different sediment layers were estimated based on the sediment accumulation rate.

2.2.2. Grain size

Grain size analysis was conducted using a laser diffraction particle size analyzer (Mastersizer 2000, Malvern Instruments Ltd., UK) with a measurement range of 0.02–2000 μm. Prior to analysis, all samples were treated with 10% H_2O_2 and 1 mol/L HCl for 24 h to eliminate OM and biogenic carbonates, and then soaked in sodium metaphosphate for 24 h. Based on the Folk classification system, grain sizes were categorized as clay (< 4 μm), silt (4–63 μm), and sand (> 63 μm). For each five samples, the test was repeated for one sample three times, with a measurement error of <3%.

2.2.3. Bulk parameters

Sediment samples were analyzed for total OC (TOC), total nitrogen (TN), and their stable isotopes according to the procedures outlined by Xing et al. (2011). After freeze-drying and homogenization, the samples were treated with 1 M HCl to eliminate inorganic carbon and subsequently rinsed multiple times with deionized water until neutralization. Measurements of TOC, TN contents, and stable isotope ratios were performed using a Thermo Flash 2000 elemental analyzer coupled with a MAT253 isotope ratio mass spectrometer. The precision of the TOC and TN determination for the sediment samples was better than ±0.03% and ± 0.01%. Reproducibility of the standard sample was better than ±0.1‰ for stable isotope ratios.

2.2.4. Lignin phenols

Lignin phenols are specific biomarkers for vascular plants. In this study, the modified alkaline CuO oxidation method (Yu et al., 2011) was employed to determine the eight major lignin phenols (Σ_8) in sediments, aiming to quantitatively evaluate the input of TOM. Approximately 1 g freeze-dried sediment, 1 g CuO, and 0.05 g $Fe(NH_4)_2(SO_4)_2{\cdot}6H_2O$ were placed into a Teflon reaction vessel, followed by the addition of 15 mL of 2 M NaOH under an N_2 atmosphere in a glove box. The vessel was then heated at 170 °C for 3 h in an incubator. After cooling, recovery standards (ethyl vanillin and trans-cinnamic acid) were introduced into the alkaline solutions, then the pH of the mixture was adjusted to 1 using HCl. The mixture was extracted three times with ethyl acetate and subsequently dried using a nitrogen blow-dry method. Derivatization was conducted prior to analysis by treating the sample with bis-(trimethylsilyl)-trifluoroacetamide (BSTFA) containing 1% trimethylchlorosilane (TMCS) at 60 °C for 1 h.

Analysis of CuO oxidation products was conducted using Thermo Trace 1300 GC instrument DB1 capillary GC column (30 m × 250 μm × 0.25 μm) containing the flame ionization detector. The oven temperature was initially held at 100 °C for 1 min, then raised to 290 °C at a rate of 4 °C/min. Helium served as the carrier gas at a constant flow rate of 1.5 mL/min. Lignin-derived compounds were identified by comparing their retention times to those of authentic standards, and quantification was performed using eight-point calibration curves.

The lignin biomarkers comprised three vanillyl (V), three syringyl (S), and two cinnamyl (C) phenols, specifically: vanillin, acetovanillone, vanillic acid; syringaldehyde, acetosyringone, syringic acid; p-coumaric acid, and ferulic acid. Additionally, three p-hydroxy phenols (P)—p-hydroxybenzaldehyde, p-hydroxyace-tophenone, and p-hydroxybenzoic acid—were included as molecular indicators. The parameters Σ8 (mg/10 g dry sediment (ds)) and Λ8 (mg/100 mg OC) represent the total concentration of the eight major lignin phenols (S + V + C) normalized per 10 g of dry sediment and per 100 mg of OC, respectively.

2.2.5. Three end-member mixing models

In this study, a three-end-member mixing model was applied to identify the sources of OC. The model utilized $\delta^{13}C$ and Λ8 as source-specific tracers and employed a Monte Carlo simulation approach to estimate the relative contributions of plant-derived OC, soil-derived OC, and marine-derived OC in core H28 (Andersson, 2011).

$$\Lambda8_{sample} = f_{plant} \times \Lambda8_{plant} + f_{soil} \times \Lambda8_{soil} + f_{marine} \times \Lambda8_{marine} \quad (2)$$

$$\delta^{13}C_{sample} = f_{plant} \times \delta^{13}C_{plant} + f_{soil} \times \delta^{13}C_{soil} + f_{marine} \times \delta^{13}C_{marine} \quad (3)$$

$$f_{plant} + f_{soil} + f_{marine} = 1 \quad (4)$$

where, f_{plant}, f_{soil}, and f_{marine} are the relative contributions of vascular plant OC, soil OC and marine OC, and the $\Lambda8_{sample}$ and $\delta^{13}C_{sample}$ are measured Λ8 and $\delta^{13}C$ values in sediment samples, respectively.

Due to the scarcity of data from the Yellow River basin, Λ8 values of typical C3 vascular plants from the Changjiang basin were adopted as a provisional end-member values (Zhao et al., 2021; Zhang et al., 2024). We acknowledge that differences in vegetation and soil properties between these basins could introduce some uncertainty. However, the application of these values is justified, as the $\delta^{13}C$ values of vascular plant OC in the Changjiang basin (−28.10 ± 1.68‰; Yu et al., 2007) fall within the range of C3 plants from the Loess Plateau (−26.7 ± 4.18‰; Wang et al., 2003), which is a major source of particulate matter in the Yellow River. Furthermore, Λ8 values in surface sediments from the Yellow Sea (0.98 ± 0.92 mg/100 mg OC) and the East China Sea (0.86 ± 0.23 mg/100 mg OC) were relatively similar (Zhang, 2012). Accordingly, the end-member values for vascular plant OC were set at $\delta^{13}C$ = −26.7 ± 4.18‰ and Λ8 = 6.00 ± 5.22 mg/100 mg OC (Wang et al., 2003). While the absolute values of source contributions are sensitive to end-member selection, we contend that the relative temporal trends are more robust, which are the primary focus of our discussion. For the soil end-member, average values from riverbank soil samples across the entire Yellow River basin were used, with $\delta^{13}C_{soil}$ = −24.86 ± 0.94‰ and $\Lambda8_{soil}$ = 2.37 ± 2.00 mg/100 mg OC (Yu et al., 2007; Gao et al., 2016). The marine OC end-member values were defined as $\delta^{13}C$ = −20.0 ± 1.0‰ and Λ8 = 0 mg/100 mg OC (Zhang et al., 2007; Wang et al., 2015).

2.2.6. Statistical analysis

Pearson correlation analysis and two-tailed significance tests were conducted with IBM SPSS Statistics 24.0 to evaluate relationships among the measured parameters. Monte Carlo simulations were implemented using a MATLAB script (Version R2020b, MathWorks) following Andersson (2011). The model incorporated end-member values of $\delta^{13}C$ and Λ8, assuming their averages and standard deviations followed a normal distribution. For each sample, 1,000,000 random values were drawn from the normal distributions of the end-member parameters—out of a total of 100,000,000 generated—and used in Eqs. 2–4. Further details regarding the simulation procedure can be found in Li et al. (2014).

3. Results

3.1. Chronology

The total and excess ^{210}Pb activities in core H28 are shown in Fig. 2. Core H28 exhibits a clear ^{210}Pb decay zone from the surface to 45 cm depth, with activity decreasing from 4.47 to 1.24 dpm/g. Below this depth, the activity of ^{210}Pb remains relatively constant. A significant correlation was observed between ln($^{210}Pb_{ex}$) and sediment depth (R^2 =

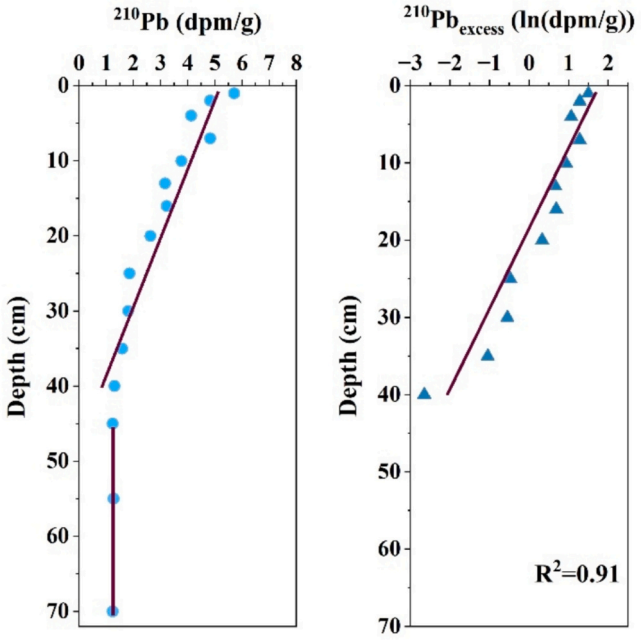

Fig. 2. Vertical distributions of ^{210}Pb activities in core H28. a, ^{210}Pb activities; b, the fitted depth curve for ln(^{210}Pb$_{ex}$).

0.91, $p < 0.01$) with the absence of surface mixing, suggesting minimal physical or biological disturbance in this core (Li et al., 2015a). Previous study has indicated that this distribution pattern is commonly observed in mud deposits, such as the western, central, and eastern mud deposits of the South Yellow Sea, the central mud deposit of the North Yellow Sea, and the central mud deposit of the Bohai Sea. The sedimentary environments, material sources, and sedimentary processes in these mud deposits have remained stable over the past century (Li et al., 2002). Based on the calculated sediment accumulation rate of 0.35 cm/yr, core H28 recorded approximately 200 years of deposition, consistent with results from nearby core C03 (35°N, 122°30′E; Cai et al., 2014).

3.2. Grain size and bulk properties

Sand, silt, and clay contents in core H28 ranged from 0.36 to 4.84%, 66.07–76.59%, and 22.55–30.48%, with mean values of 1.13 ± 0.86%, 72.04 ± 1.86%, and 26.83 ± 1.75%, respectively (Fig. 3a). The mean grain size varied between 6.74 and 8.77 μm, averaging 7.67 ± 0.43 μm (Fig. 3b). From 70 to 45 cm, the mean grain size exhibited a fluctuating fining trend, characterized by increasing clay content, decreasing sand content, and variable silt content. Between 45 and 22 cm, the sediments gradually coarsen, with declining clay content, increasing sand content, and silt content showing strong fluctuations but an overall upward trend. Above 22 cm, the mean grain size displayed a variable coarsening pattern, accompanied by decreasing clay content, increasing sand content, and silt content that fluctuates markedly yet generally increases.

TOC and TN contents in core H28 ranged from 0.60 to 1.10% and 0.10–0.16%, with average values of 0.86 ± 0.12% and 0.13 ± 0.01%, respectively (Fig. 3c, d). The TOC content showed a decreasing trend from 70 to 60 cm, followed by a gradual increase above 60 cm, with a more pronounced rise beyond 25 cm (Fig. 3c). In contrast, TN content exhibited a consistent upward trend from the bottom to the top of the core, with a notably stronger increase above 25 cm (Fig. 3d). A significant positive correlation was observed between TOC and TN ($r = 0.88$, $p < 0.001$), and their similar vertical distribution patterns suggested a common origin (Fig.S1a).

The δ^{13}C values and C/N ratios in core H28 ranged from −23.62‰ to −22.32‰ and 6.19 to 8.71, with average values of −23.04 ± 0.32‰ and 7.45 ± 0.51, respectively (Fig. 3e, f). The δ^{13}C values showed considerable fluctuation between 70 and 60 cm, with an overall shift toward more positive values. From 60 to 50 cm, they gradually became more positive, whereas between 50 and 20 cm, a consistent trend toward more negative values was observed, reaching the most negative values in the core, before shifting back toward positive values toward the top (Fig. 3e). The C/N ratios decreased between 70 and 60 cm, then gradually increased from 60 to 10 cm, and finally decreased from 10 cm toward the top (Fig. 3f). A negative correlation was observed between δ^{13}C values and C/N ratios ($r = -0.52$, $p < 0.001$), indicating that both proxies are useful for identifying the sources of OM (Fig.S1b). However, since their trends are not entirely consistent, caution should be exercised when selecting source indicators.

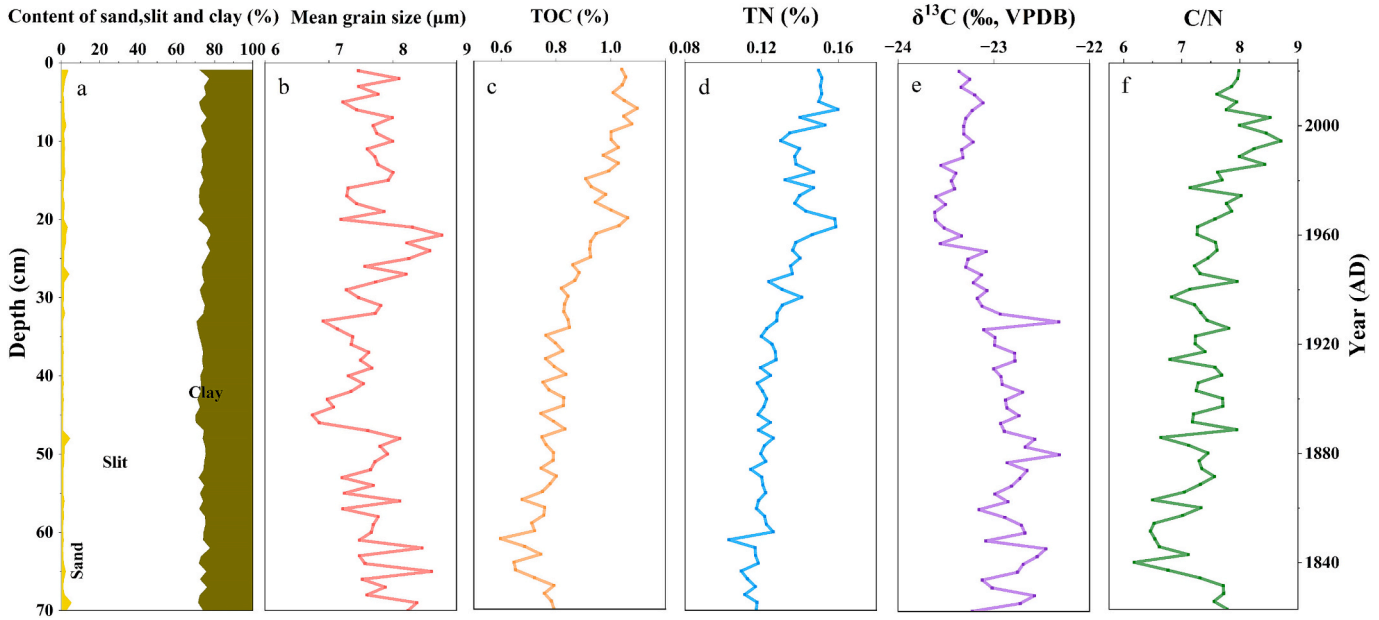

Fig. 3. a, Content of sand, slit and clay (%); b, mean grain size (μm); c, TOC content (%); d, TN content (%); e, δ^{13}C (‰, VPDB); f, C/N ratios in core H28.

3.3. Lignin phenols

The Σ8 values in core H28 ranged from 0.16 to 0.50 mg/10 g ds, with an average of 0.27 ± 0.08 mg/10 g ds (Fig.S2a). The Σ8 values remained relatively low at the bottom of the core (70–50 cm), followed by a consistent increasing trend from 50 to 20 cm, reaching the highest value in the core around 20 cm. Thereafter, Σ8 showed a continuous decrease from 20 cm upward, with relatively low values observed in the top 5 cm. The Λ8 values in core H28 ranged from 0.19 to 0.49 mg/100 mg OC, with an average of 0.31 ± 0.07 mg/100 mg OC (Fig.S2b). The Λ8 values were relatively low at the bottom of the core (70–50 cm), occasionally interrupted by fluctuating higher values. A sustained increasing trend was observed from 50 to 20 cm, reaching the maximum value around 20 cm, followed by a continuous decrease upward. The top 5 cm also exhibited relatively low Λ8 values. The vertical distribution patterns of Σ8 and Λ8 were generally similar and show a strong positive correlation (Fig. S3a; $r = 0.90$, $p < 0.001$). This suggests that lignin and other OM in the core may have been influenced by similar environmental factors during deposition—such as microbial degradation, resulting in no significant post-depositional alteration in the ratio of lignin content to TOC content in the sediment (Hedges et al., 1988).

Overall, the S phenols showed the highest abundance, followed by non-lignin phenols (P) and V phenols, while the C phenols had the lowest concentrations (Fig. S4a–d). The P phenols ranged from 0.06 to 0.25 mg/10 g ds, with an average of 0.12 ± 0.04 mg/10 g ds (Fig. S4a). The S, V, and C phenols exhibited concentration ranges of 0.07–0.26 mg/10 g ds, 0.05–0.19 mg/10 g ds, and 0.02–0.06 mg/10 g ds, with mean values of 0.13 ± 0.04 mg/10 g ds, 0.10 ± 0.03 mg/10 g ds, and 0.04 ± 0.01 mg/10 g ds, respectively (Fig. S4b–d).The Pon/P ratio ranged from 0.22 to 0.50, with an average of 0.34 ± 0.06 (Fig. S2c), indicating a relatively high proportion of lignin-derived OM within the P phenols (Houel et al., 2006).

The S/V and C/V ratios ranged from 1.00 to 1.86 (Fig. S2d) and 0.20–0.60 (Fig. S2e), with mean values of 1.32 ± 0.17 and 0.37 ± 0.11, respectively. Their vertical distributions exhibited similar trends (Fig. S3b; $r = 0.61$, $p < 0.001$). The LPVI values ranged from 159 to 1149, with an average of 446 ± 226 (Fig. S2f). LPVI values showed strong positive correlations with both S/V (Fig. S3c; $r = 0.76$, $p < 0.001$) and C/V (Fig. S3d; $r = 0.96$, $p < 0.001$). Overall, the S/V, C/V, and LPVI values in core H28 displayed a fluctuating decreasing trend, with relatively higher values observed in the 70–50 cm interval.

$(Ad/Al)_V$ and (Ad/Al)s represent the acid-to-aldehyde ratios of V and S phenols, respectively (Hedges et al., 1988; Dittmar and Lara, 2001). These ratios are used to assess the degradation or diagenetic state of lignin tissues. In core H28, $(Ad/Al)_V$ and (Ad/Al)s showed a positive correlation (Fig. S3e; $r = 0.34$, $p < 0.05$). The $(Ad/Al)_V$ ratio ranged from 0.36 to 0.85, with a mean of 0.48 ± 0.07. It exhibited little variation throughout the core, with occasional fluctuating high values (Fig. S4e). The (Ad/Al)s ratio ranged from 0.42 to 0.89, with a mean of 0.61 ± 0.10 (Fig. S4e). Values were relatively high between 70 and 40 cm, showing an initial increase followed by a decrease, and remained relatively stable below 40 cm (Fig. S4e).

3.4. Source and degradation of OM

Bulk OM properties, such as $\delta^{13}C$ values and C/N ratios, are frequently utilized to characterize the sources of OM. TOM typically exhibits more negative $\delta^{13}C$ values and higher C/N ratios compared to MOM. Marine algae have C/N ratios ranging from 4 to 10 (Meyers, 1994), while C3 plants generally have C/N ratios of approximately 12 or higher (Tyson, 1995), and C4 plants typically exhibit C/N ratios of 30 or more (Meyers, 1994). The $\delta^{13}C$ values of marine algae range from −19‰ to −21‰ (Fry and Sherr, 1984). In contrast, C3 and C4 plants have $\delta^{13}C$ values that fall within the ranges of −24‰ to −32‰ and − 9‰ to −17‰, with average values of −27‰ and − 13‰, respectively (Meyers, 1997; Lamb et al., 2006). In core H28, the observed C/N ratios (6.19–8.71) suggest that OM in the sediments was predominantly derived from marine algae (Fig. 4a). However, the $\delta^{13}C$ values (−23.62‰ to −22.32‰) indicate a mixed origin of the sedimentary OC, with a predominance of marine sources (Fig. 4a). It indicates that these two proxy indicators identify different sources of OM in this marine region. The accurate quantification of OM sources using the C/N ratio method is challenging due to the diversity of material sources, the complexity of depositional environments, and the potential overprint of geological processes (Hedges et al., 1997; Blair and Aller, 2012). For example, degradation by terrestrial soil microorganisms can reduce the C/N ratio (Meyers, 1997). Therefore, greater caution should be taken when selecting source proxies. Notably, the absence of a significant correlation between TOC content, mean grain size ($r = 0.07$, $p > 0.05$), sand content ($r = 0.21$, $p > 0.05$) and clay content ($r = -0.10$, $p > 0.05$) in core H28 may indicate that the preservation and input of OM outweigh the sole control of hydrodynamic sorting (Hedges and Keil, 1995; Gordon and Goñi, 2003). OC in core H28 is derived from both terrestrial and marine sources, whose contributions may respond differently to grain size variations, thereby complicating the establishment of a simple, singular correlation.

The S/V and C/V ratios, along with LPVI values, are employed to characterize the sources of vegetation within the basin. S/V is used to distinguish lignin from gymnosperms (~0) or angiosperms (0.6–40); C/V is used to distinguish nonwoody tissues (> 0.20) from woody tissues (< 0.05; Goñi et al., 1998; Bianchi, 2011). In core H28, the S/V and C/V ratios ranged from 1.00 to 1.86 and 0.20–0.60 (Fig. 4b), with mean values of 1.32 ± 0.17 and 0.37 ± 0.11, indicating that nonwoody angiosperm tissues dominate TOM in this study (Fig. 4b). The LPVI values of core H28 ranged from 159 to 1149, with a mean value of 446 ± 226 (Fig. S2f), suggesting that nonwoody angiosperm tissues were the predominant component of TOM in core H28, which is consistent with the interpretation based on the S/V and C/V ratios. However, the interpretation of these lignin vegetation parameters may be influenced by pollen input and hydrodynamic sorting processes. Given that core H28 is located in a nearshore marine environment (Fig. 1), its TOM is primarily transported from coastal areas rather than direct input, rendering it vulnerable to hydrodynamic sorting. During this process, most fine-grained sediments are transported to the nearshore region, where fine particles are predominantly associated with nonwoody angiosperm tissues, potentially leading to an overestimation of the contribution from nonwoody angiosperms.

The three-end-member model results indicate that vascular plant-derived OM accounted for 8.87–14.93%, with an average of 12.29 ± 1.48% (Fig. 5b); soil-derived OM accounted for 26.24–45.36%, with an average of 37.21 ± 4.65% (Fig. 5b); and marine-derived OM accounted for 35.11–60.29%, with an average of 49.50 ± 6.13% (Fig. 5c). Prior to 1880, both the $\delta^{13}C$ values and the contribution of TOM (plant-derived and soil-derived OM) exhibited fluctuating trends (Fig. 5a, b). Thereafter, from 1880 to 1970, the $\delta^{13}C$ values shifted toward more negative values, and the contributions from both plant-derived and soil-derived OM gradually increased, with the increase in soil-derived OM contribution being more pronounced (Fig. 5b). The TOM contribution reached its maximum around 1970 (Fig. 5b). Finally, after approximately 1970, the $\delta^{13}C$ values shifted toward more positive values, and the contribution of TOM showed a declining trend (Fig. 5c).

The ratios of $(Ad/Al)_V$ and $(Ad/Al)_S$ are usually used to characterize the degradation of lignin tissues, and their values increase as the degree of microbial degradation increases. In this core, $(Ad/Al)_V$ and $(Ad/Al)_S$ ratios ranged from 0.36 to 0.85 and 0.42 to 0.89, with a mean value of 0.48 ± 0.07 and 0.61 ± 0.10 (Fig. 5d). These values indicated that TOM in this core has undergone moderate degradation. The generally consistent distribution trends of $(Ad/Al)_S$ and $(Ad/Al)_V$ reflect similar major degradation pathways for both phenols. Furthermore, the higher $(Ad/Al)_S$ values compared to $(Ad/Al)_V$ suggested a greater degree of degradation in the S phenols than in the V phenols, which may be attributed to the fact that S phenols are more susceptible to diagenetic

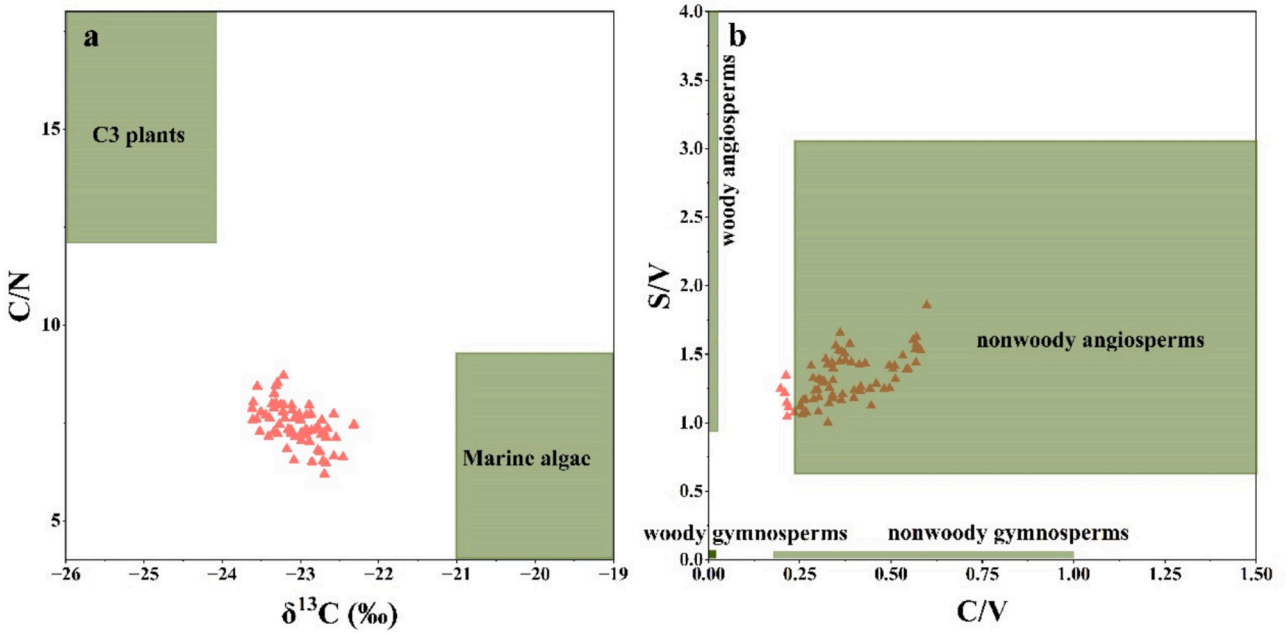

Fig. 4. a, $\delta^{13}C$ versus C/N ratio for all samples of core H28, where the background labels of OM sources are according to Fry and Sherr (1984), Meyers (1994), Tyson (1995) and Lamb et al. (2006); b, C/V versus S/V ratios for all samples of core H28, where the typical ranges of different vegetation types are from Goñi et al. (1998), Bianchi (2011).

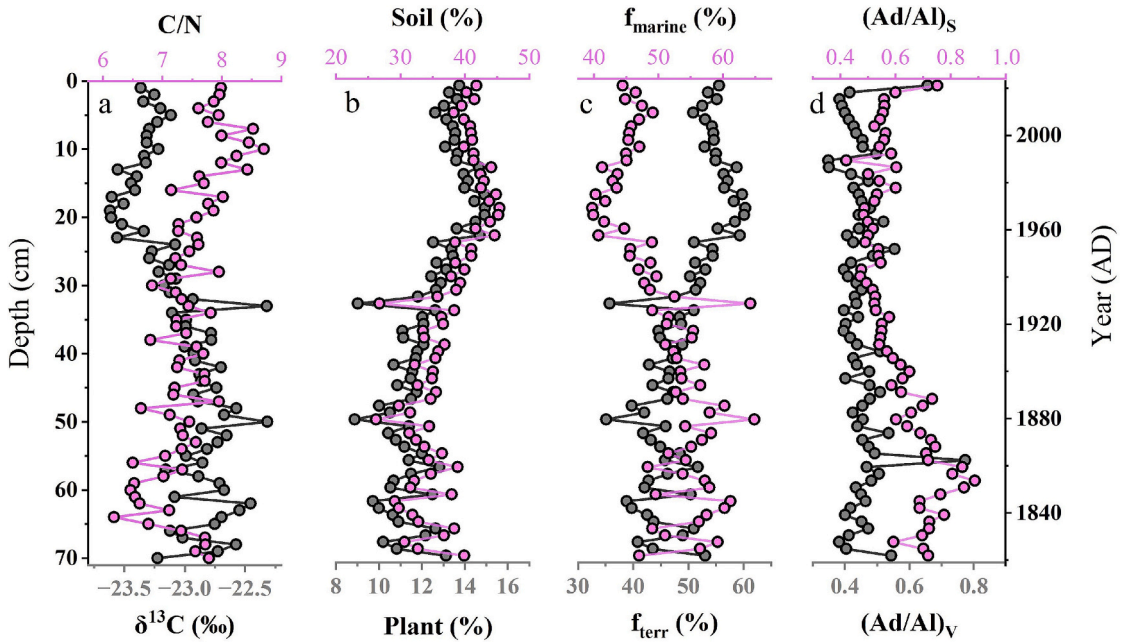

Fig. 5. Variations of OM proportions and degradation parameters in core H28. a, $\delta^{13}C$ values (grey line) and C/N (pink line) of core H28; b, plant OM fraction (grey line) and soil OM fraction (pink line) of core H28; c, terrestrial OM fraction (f_{terr}; f_{plant} and f_{soil}) (grey line) and marine OM fraction (pink line) of core H28; d, $(Ad/Al)_V$ ratios (grey line) and $(Ad/Al)_S$ ratios (pink line) of core H28. (For interpretation of the references to colour in this figure legend, the reader is referred to the web version of this article.)

degradation than V phenols (Huang et al., 1999).

4. Discussion

4.1. Impact of centennial climate change on the fate of OM in the South Yellow Sea

In the South Yellow Sea, sediment transport and deposition are primarily driven by sediment supply and depositional environment dynamics (Zhou et al., 2015). Between 1950 and 1970, core H28 exhibited high values of mean grain size, sand content, TOC content, Σ8 content, and TOM contribution (Fig. 6a–e), corresponding to a period of intensified EAWM (Shi and Yang, 1998; Zhang, 2005). Based on statistical difference tests, we found that the mean grain size (8.17 μm), TOC content (0.97%), Σ8 content (0.43 mg/10 g ds), and TOM contribution (56.97%) during the strong EAWM period were significantly higher than those in other periods ($p < 0.05$). Crucially, the intensity of the YSWC and YSCC, which is modulated by the EAWM, exerts a dominant control

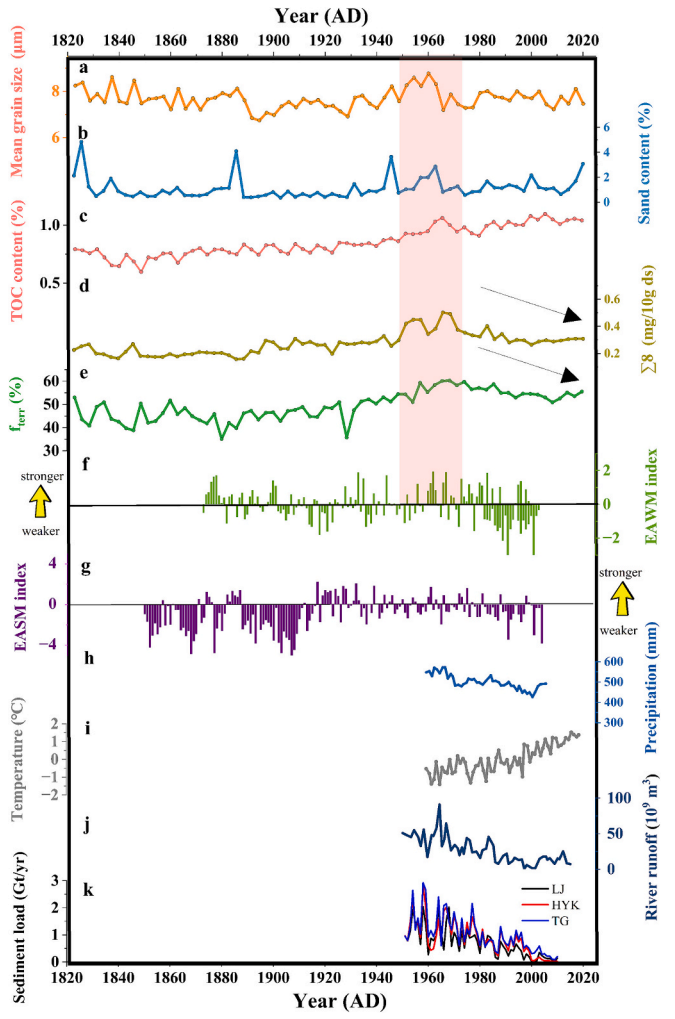

Fig. 6. Records of grain size, TOC and lignin phenols of core H28 and their correspondence with climate indicators during 1820–2023. a, Mean grain size of core H28 (μm); b, sand content of core H28 (%); c, TOC content of core H28 (%); d, Σ8 of core H28 (mg/10 g ds); e, terrestrial OM contribution of core H28 (%); f, EAWM index (Shi and Yang, 1998; Zhang, 2005); g, EASM index (IPCC, 2007); h, Annual precipitation in the whole Yellow River basin during 1957–2006 (Huang et al., 2009); i, Trends of annual average temperature of Yellow River source area from 1960 to 2019 (Liu et al., 2021); j, Annual river runoff recorded at Lijin Station from 1950 to 2016 (data from the Yellow River Conservancy Commission); k, The time series of annual sediment load at the main gauging stations along the Yellow River basin; TG, Tongguan; HYK, Huayuankou; LJ, Lijin (Wang et al., 2016). (For interpretation of the references to colour in this figure legend, the reader is referred to the web version of this article.)

on the fate of TOM by facilitating its advection and sequestration through the resuspension and subsequent redistribution of fine-grained particles (Goñi and Hedges, 1995; Zhou et al., 2015). The strengthened EAWM enhanced the southward transport of resuspended sediments, delivering more TOM to the South Yellow Sea. In addition, an intensified Kuroshio intrusion transported nutrient-rich subsurface water to coastal areas and strengthened vertical mixing in the water column (Xu et al., 1999; Shi et al., 2010), leading to increased marine primary productivity during this period (Xing et al., 2016). The rise in primary productivity inevitably promoted the OC accumulation in sediments, resulting in higher TOC content (Fig. 6c).

It is noteworthy that both Σ8 content and TOM contribution showed a continuous declining trend after approximately 1970 (Fig. 6d, e), which aligns with the reduction in natural runoff and sediment load of the Yellow River since around the 1970s (Fig. 6j, k). Annual runoff recorded at the Lijin Station decreased sharply from around 1970 (Fig. 6j). River runoff is influenced by many factors, with annual precipitation likely being the most significant (Wu et al., 2017). The upper and middle reaches of the Yellow River are located in arid and semi-arid regions with low annual precipitation (< 150 mm/yr), while the lower reaches are more humid, receiving over 900 mm/yr (Chen et al., 2005). From 1985 to 2000, the average annual precipitation across the Yellow River Basin was only 427.8 mm, approximately 10% lower than that before the 1960s. Prior to the 1970s, precipitation in the basin exhibited strong interannual variability (> 216 mm), which subsequently moderated. Most previous studies attribute the declining trend in precipitation across the Yellow River Basin to changes in ENSO activity and the intensity of the EASM over recent decades (Fig. 6g, h; Xu, 2003; Wang et al., 2006a; Wang et al., 2007; Huang et al., 2009; Yang et al., 2011).

In addition to reduced precipitation, global climate change such as global warming has also impacted the hydrological cycle of the Yellow River Basin. Since 1970, the average annual temperature in the basin has risen from 16.5 °C to 17.5 °C (Xu, 2005), while regional precipitation has shown a contrasting decreasing trend. Hao et al. (2006) noted that the temperature in the source region of the Yellow River increased at a rate of 0.31 °C per decade from 1954 to 2007. Liu et al. (2021) found that the annual average, maximum, and minimum temperatures in the source region all exhibited consistent upward trends from 1960 to 2019 (Fig. 6i). Consequently, the climate in the Yellow River Basin has become warmer and drier, leading to increased agricultural evapotranspiration and reservoir evaporation (Zhang et al., 2004), reduced river flow, and higher demand for agricultural irrigation water. Ultimately, high evaporation combined with reduced freshwater recharge has decreased the natural runoff of the Yellow River, thereby contributing to a reduction in fluvial sediment load.

As the primary sink for sediments delivered by the Yellow River, changes in its sediment discharge into the sea are bound to affect the fate of OM in the South Yellow Sea, leaving corresponding depositional records. Historically, the Yellow River has been one of the largest transporters of riverine sediment; however, over the past 60 years, it has experienced a reduction of approximately 90% in its sediment load. Climate change and human activities have collectively altered soil erosion and sediment transport processes in the basin (Frangipane and Paris, 1994; Glazyrin and Tashmetov, 1995; Lu and Higgitt, 1998; Wang et al., 2025). During this period, climate change (rising temperatures and decreasing precipitation) may account for 10%–20% of the reduction in sediment discharge into the sea, while the remaining 80%–90% is attributed to human activities within the basin (Wang et al., 2007; Wang et al., 2016; Wu et al., 2020). In Section 4.2, we will further discuss the impact of centennial-scale human activities on the fate of OM in the South Yellow Sea.

4.2. *Impact of centennial human activities on the fate of OM in the South Yellow Sea*

Before 1970, Σ8 content and TOM contribution exhibited relatively high values and increasing trend (Fig. 7b, c). The Western Industrial Revolution spread to China around the 1860s, significantly stimulating the Chinese economy. By 1860, the population of the Loess Plateau had already exceeded 40 million and continued to grow at an accelerating rate. Cultivation and deforestation driven by rapid population growth have diminished forest cover, accelerated soil erosion, and consequently lead to a gradual increase in the sediment load of the Yellow River, with relatively high level of around 1.31 Gt/yr with fluctuations over the century (Ren and Zhu, 1994; Saito et al., 2001; Wu et al., 2020). This process ultimately contributed to an increase in TOM input during this period (Zhang et al., 2024). Subsequently, the population of the Loess Plateau quadrupled, reaching 104 million by the year 2000 (Fig. 7d; Wang et al., 2006b).

However, since around 1970, $\delta^{13}C$ values have shifted toward more

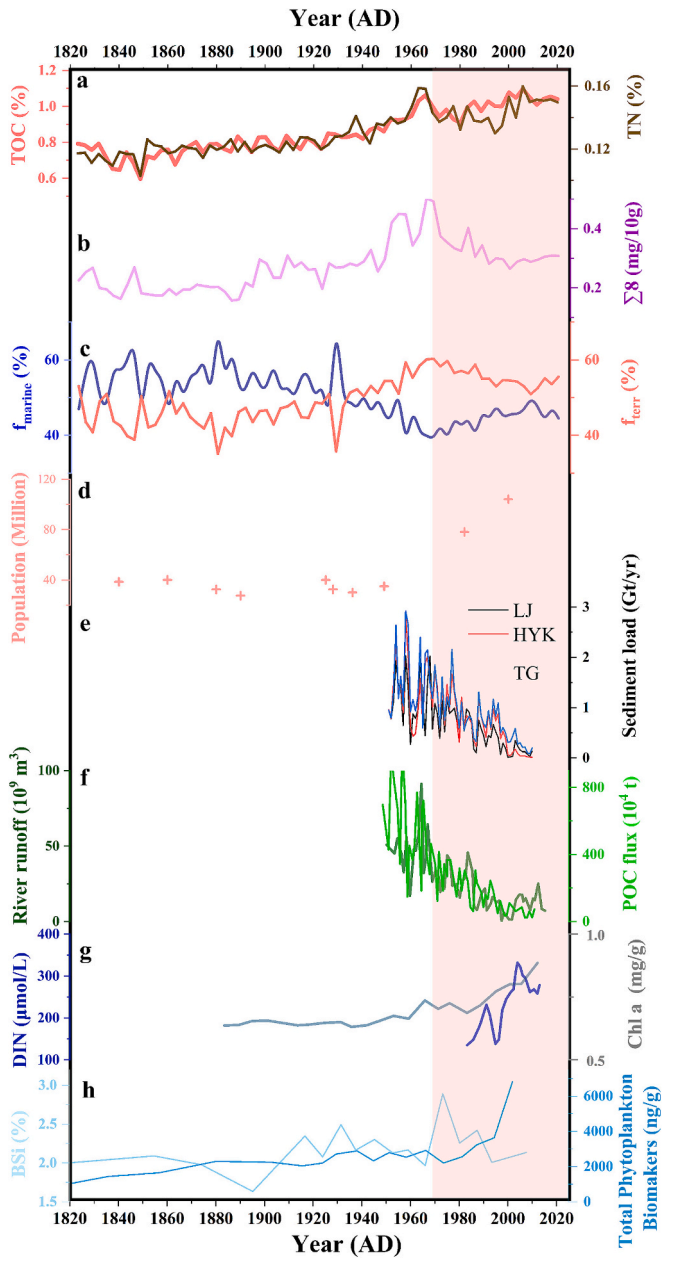

Fig. 7. Records of TOC, lignin phenols, terrestrial and marine OM contribution of core H28 and their correspondence with human activity indicators during 1820–2023. a, TOC (red line) and TN (brown line) of core H28 (%); b, Σ8 of core H28 (mg/10 g ds); c, Terrestrial (red line) and marine OM contribution (blue line) of core H28 (%); d, Population changes in the Loess Plateau over the past decades (Wang et al., 2016); e, The time series of annual sediment load at the main gauging stations along the Yellow River basin; TG, Tongguan; HYK, Huayuankou; LJ, Lijin (Wang et al., 2016); f, Annual river runoff recorded at Lijin Station from 1950 to 2016 (dark green line; data from the Yellow River Conservancy Commission) and POC flux at Lijin Station from 1950 to 2016 (light green line; the calculation methods for POC flux in the Yellow River were published by Zhang et al. (2009) and Zhu et al. (2012), and data were obtained from Wang and Chen (2009) and the YRCC); g, Inter-annual variation in concentration of DIN in the Yellow River (blue line; Wang et al., 2018) and Chl a concentration in the C03 sediment core of the South Yellow Sea (grey line; Cai et al., 2014); h, BSi (Yang et al., 2015) and phytoplankton biomarkers (Xing et al., 2009) in sediments of the central Yellow Sea mud deposit. (For interpretation of the references to colour in this figure legend, the reader is referred to the web version of this article.)

positive values, accompanied by a gradual decrease in Σ8 content and TOM contribution (Fig. 7b, c). This trend is consistent with the phased decline in sediment load from the Yellow River (Fig. 7e). Simultaneously, the annual particulate OC (POC) flux at the Lijin Station near the Yellow River estuary decreased by nearly 90% in the 21st century compared to the 1950s (Fig. 6f), aligning with the trend in sediment load. Notably, the declining trend of Σ8 content and TOM contribution has significantly slowed since around 2000s (Fig. 7b, c). This pattern closely corresponds with the trends in sediment load and runoff of the Yellow River, which entered a stable low-value plateau phase after 2000, exhibiting no further significant decline.

The reduction in sediment load of the Yellow River since around 1970 has been influenced by intensified human activities, including dam construction, soil and water conservation measures, and increased water consumption (Nilsson et al., 2005; Syvitski et al., 2005). By 2001, a total of 3147 reservoirs had been built in the Yellow River Basin, with a total storage capacity of 57.4×10^9 m^3, nearly equivalent to the basin's average annual natural runoff (Zhang et al., 2001). The major reservoirs along the main stream (Sanmenxia, Liujiaxia, Longyangxia, and Xiaolangdi) gradually reduced sediment delivery (Fuggle et al., 2000). In the late 1950s, a series of soil and water conservation measures were implemented to mitigate the erosive impact of heavy rainfall in the Loess Region, maintain land productivity, and improve environmental quality. These practices included building terraces and sediment-trapping dams, reforestation and grass planting to improve land cover, and establishing grazing land. These measures reduced mid-basin sediment yield by 0.25–0.30 Gt per year, accounting for about 40% of the total sediment reduction attributable to human activities (Walling and Fang, 2003; Huang and Zhang, 2004). Meanwhile, rapid population growth and economic development have drastically increased water demand, primarily for agricultural irrigation, which accounts for over 92% of total water use in the basin (Yang et al., 1998). As a result, the Yellow River's discharge to the sea has declined steadily since the 1950s, leading to severe flow interruptions in the lower reaches—peaking at 226 flow interruptions days in 1997 (Xu, 2004). Although reservoir regulation alleviated the extreme flow interruptions events after 1997, the average annual water discharge into the sea in the 1990s was only 28.7% of that in the 1950s, and sediment discharge fell to 29.5% of the mid-century level (Wang et al., 2006a). This sharp decline in river flow has led to a continued reduction in sediment input to the sea (Wang et al., 2006a).

A fundamental challenge in marine sedimentology is the limited spatial representativeness of individual sediment core, which primarily capture localized processes. To move beyond site-specific interpretations and robustly assess the sedimentological response of the eastern China marginal seas to anthropogenic and climatic forcings, we therefore adopted a multi-core approach. This study integrates data from 9 sediment cores, strategically collected from mud deposit and distal shelf in eastern China marginal seas (Fig. 1; Table S1; Li et al., 2015a; Li et al., 2015b; Chen et al., 2017; Sun et al., 2020; Xiao et al., 2020; Wang et al., 2021). Recent studies have documented substantial declines in both water discharge and sediment flux from numerous river systems to the global oceans over the past few decades: including the Colorado, Mississippi, Indus, Nile, Yangtze, and Yellow Rivers (Meade and Parker, 1985; Stanley and Warne, 1998; Yang et al., 1998; Walling and Fang, 2003; Wang et al., 2006a; Yang et al., 2006). This raises a critical question for the eastern China marginal seas: has this well-documented decline in riverine sediment supply translated into a measurable and synchronous decline in the burial flux of TOM in the marine sediment? By comparing high-resolution TOM records from multiple cores, we indeed observe a pervasive declining trend in recent decades (Fig. 8). However, the onset of this decline in TOM varies, though it mostly occurred between the 1960s and 1980s (Fig. 8). We propose that this spatial heterogeneity is not merely due to analytical uncertainties but likely reflects the interplay of multiple factors. The sediment reduction histories differ between the Yellow River and Changjiang River in both timing and magnitude (Sun et al., 2020; Xiao

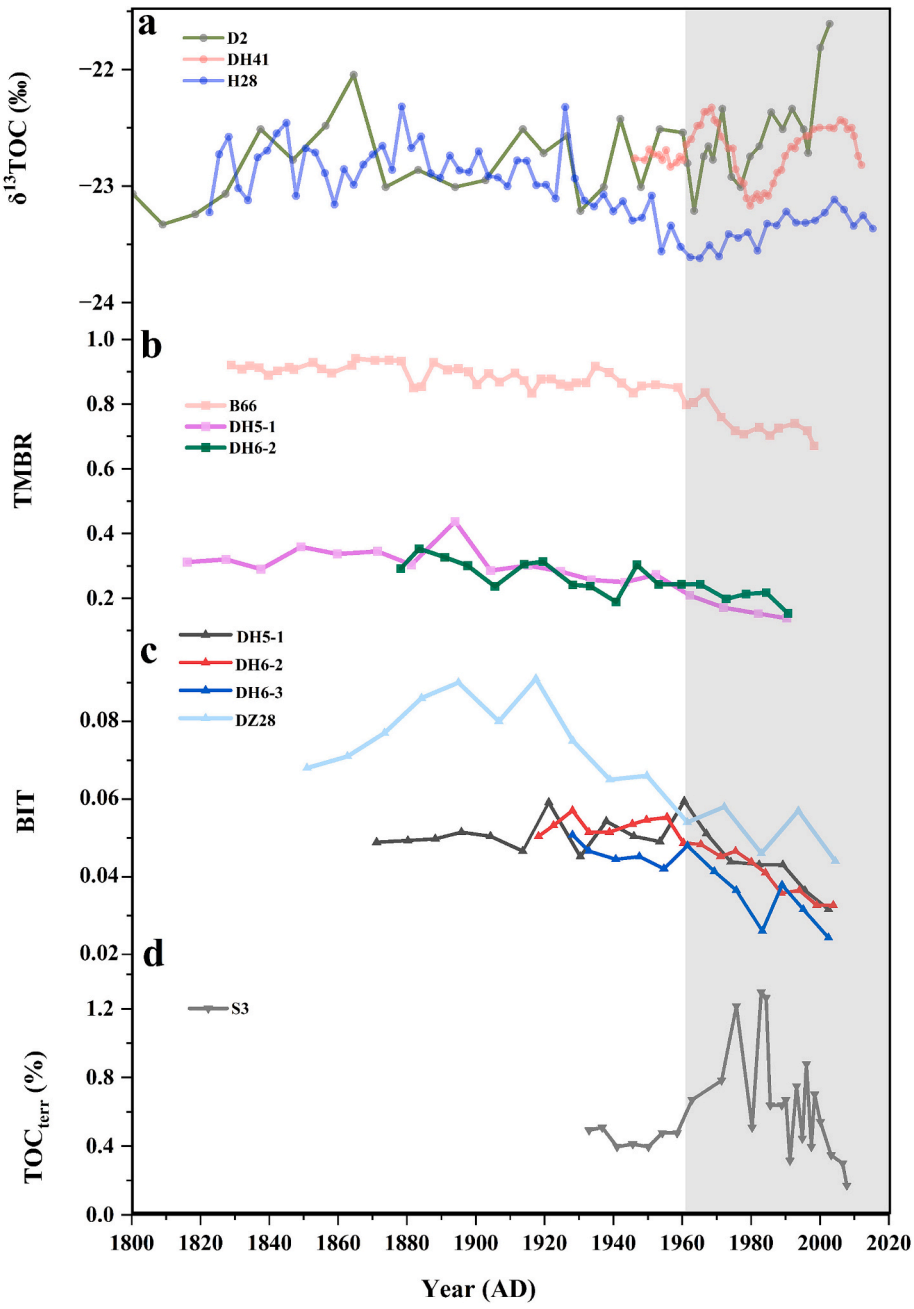

Fig. 8. Response of the cores in Eastern China marginal sea to human activities on a century scale. a, $\delta^{13}C_{TOC}$ of D2 (Li et al., 2015a), DH41 (Sun et al., 2020) and H28 (this study) cores; b, TMBR index of B66 (Xiao et al., 2020), DH5–1 (Cao et al., 2017) and DH6–2 (Cao et al., 2017); c, BIT index of DH5–1 (Cao et al., 2017), DH6–2 (Cao et al., 2017), DH6–3 (Cao et al., 2017) and DZ28 (Chen et al., 2017) cores; d, Terrestrial TOC content of S3 core (Li et al., 2015b).

et al., 2020). Besides, upon entering the ocean, sediments are redistributed by currents to form distinct mud deposits, with signal transmission along these pathways potentially causing time lags or smoothing in distal records (Liu et al., 2007). Moreover, variations in sedimentation rates and benthic community activity between sites can modulate the preservation and dilution of the TOM signal (Aller, 2013).

Notably, unlike the declining trends in both Σ8 content and TOM contribution observed around 1970, TOC and TN content consistently maintained an increasing trend (Fig. 7a). It is noteworthy that around 1970, the grain size parameters of the sediments (such as mean grain size and sand content) did not exhibit significant abrupt changes (Fig. 3a, b), indicating relatively stable sedimentary conditions during this period. This suggests that the observed increase in MOM contribution (Fig. 7c) more likely to reflect changes in source input rather than alterations induced by sedimentary dynamic processes. Since the 1970s, increased fertilizer application and wastewater discharge have introduced substantial nutrients into the estuary region. The concentration of dissolved inorganic nitrogen in the Yellow River increased slowly in the early 1980s, rose rapidly from the mid-1980s to the early 2000s, and has since remained high with fluctuations, reaching levels in the estuary during the 1990s that were four times those of the 1950s (Fan and Huang, 2008). Since the 1980s, chlorophyll-a concentrations in the Yellow River estuary and adjacent coastal waters have generally shown an upward trend (Tang et al., 2003; Wu et al., 2016), indicating significantly enhanced marine productivity. Furthermore, from 1980 to 2007, with increasing nitrogen nutrients, primary productivity in the south of the Shandong Peninsula approximately doubled, and the average chlorophyll-a concentration increased from 0.7 mg/m^2 in 1950 to about

2.2 mg/m^2 in 2007 (Yang et al., 2015). Over the past two decades, rapid coastal economic development, expansion of aquaculture, sharp population growth, intensified agricultural activities, and widespread fertilizer use have led to significant increases in TN and total phosphorus concentrations in seawater (Qu et al., 2018). These changes have promoted phytoplankton growth and contributed to the continuous rise in TN content in core H28 (Fig. 7a). Population growth in the Yellow River and Changjiang River basins, the use of artificial nitrogen and phosphorus fertilizers, and anthropogenic emissions of trace elements may have further enhanced riverine nutrient supplies to marine phytoplankton, leading to increasingly severe eutrophication issues in the coastal areas of the eastern China marginal Sea (Duan et al., 2014; Yang et al., 2015).

4.3. OC accumulation rate in the South Yellow Sea on a centennial scale

The mass accumulation rate and OC accumulation rate of core H28 were calculated based on measurements of TOC content, sediment dry density, and the sediment accumulation rate derived from ^{210}Pb dating. The mass accumulation rate of core H28 ranged from 0.34 to 0.41 g cm^{-2} yr^{-1}, with a mean value of 0.37 ± 0.02 g cm^{-2} yr^{-1}. The OC deposition rate ranged from 23.27 to 42.93 g C m^{-2} yr^{-1}, with a mean value of 32.02 ± 4.19 g C m^{-2} yr^{-1} (Fig. 9). These values are close to Bohai Sea (27 g C m^{-2} yr^{-1}; Hu et al., 2016), slightly lower than those reported for the East China Sea (41.2 g C m^{-2} yr^{-1}; Sun et al., 2020), but slightly higher than those of the Baltic Sea (18–35 g C m^{-2} yr^{-1}; Winogradow and Pempkowiak, 2014), the Louisiana Inner Continental Shelf (22.7 g C m^{-2} yr^{-1}; Gordon et al., 2001), and the Arabian Sea (0.8–21.0 g C m^{-2} yr^{-1}; Bhushan et al., 2001). Furthermore, the mean OC deposition rate of this core is approximately 8 times higher than the global average for shelf sediments (4.15 g C m^{-2} yr^{-1}; Berner, 1982). Considering the area of the South Yellow Sea Central mud deposit (99.3 × 10^3 km^2; Qiao et al., 2017), it can be estimated that the OC deposited within South Yellow Sea Central mud deposit sediments should have been 3.18 Mt/yr, accounting for 3% of global shelves (Table 1). The high OC deposition rate and flux indicate that the South Yellow Sea Central mud deposit serves as a significant global sink of sedimentary OC and plays an important role in the global OC cycle.

In core H28, a strong positive correlation exists between the OC deposition rate and TOC content ($r = 0.95$, $p < 0.001$; Fig. S5a), while no significant correlation is observed with the mass accumulation rate ($r = -0.12$, $p > 0.05$; Fig. S5b) or sediment bulk density (r = −0.12, $p > 0.05$; Fig. S5c). This indicates that the OC deposition rate in the study area is may primarily controlled by TOC content. It is noteworthy that after approximately 1970, although the mass accumulation rate showed a significant declining trend due to reduced sediment discharge, the OC deposition rate exhibited a fluctuating but gradually increasing pattern (Fig. 9), which may be largely attributed to enhanced marine productivity and elevated TOC content. This interpretation is consistent with previously established productivity reconstructions for the Yellow Sea. The elevated biogenic silica levels observed post-1950s indicate a significant increase in primary productivity in the Yellow Sea during this period (Fig. 7h; Yang et al., 2015). This trend is further supported by sedimentary lipid biomarker records that reveal heightened phytoplankton productivity following the 1960s (Fig. 7h; Xing et al., 2009). The increase in primary productivity would have facilitated enhanced vertical export and subsequent burial of OC from surface waters. Therefore, the variation in OC deposition rates in the South Yellow Sea is likely intrinsically linked to changes in productivity over these timescales.

Table 1
OC deposition rate and fluxes reported in other studies globally.

region	OC deposition rate (g C m^{-2} yr^{-1})	OC deposition flux (Mt/yr)	Reference
Zhejiang-Fujian Mud Zone	41.2	2.54	Sun et al., 2020
Bohai sea	27	2.0	Hu et al., 2016
Baltic Sea	18–35	1.955	Winogradow and Pempkowiak, 2014
Louisiana Inner Continental Shelf	22.7	0.18	Gordon et al., 2001
Arabian Sea	0.8–21.0		Bhushan et al., 2001
South Yellow Sea Central mud deposit	32.02	3.18	This study
Global shelves	4.15	108	Berner (1982)

5. Conclusions

Using the bulk properties and lignin phenol index of H28 sediment core in the South Yellow Sea, this study has discussed the variations of terrestrial organic matter burial in the past two centuries, and linked its variability to climate change and human activities in the Yellow River Basin. Nonwoody angiosperms dominated the terrestrial organic matter, and terrestrial organic matter in this core underwent a moderate degradation. We found that enhanced East Asian winter monsoons increased the southward transport of resuspended sediments between 1950 and 1970, leading to more terrestrial organic matter being

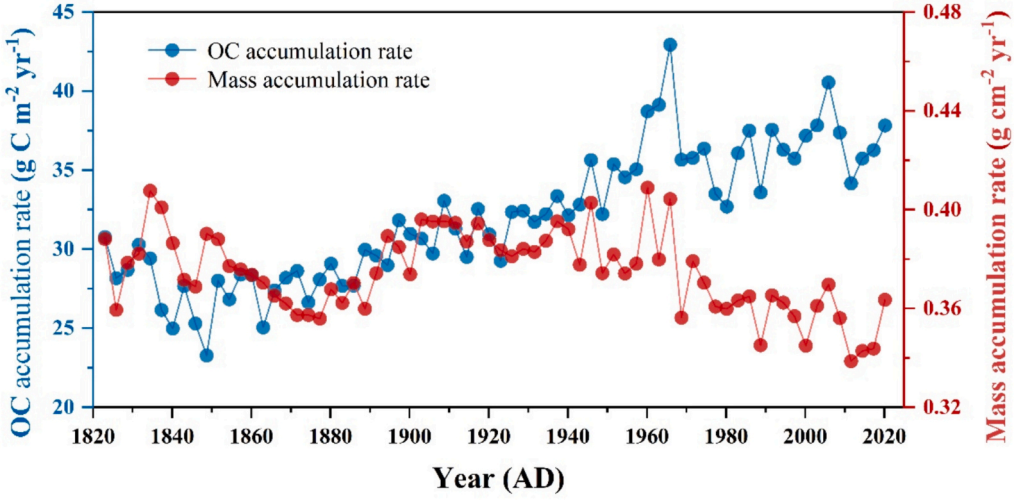

Fig. 9. Changes of estimated mass accumulation rate and OC accumulation rate in core H28.

transported to the South Yellow Sea. Furthermore, rising temperatures with reduced precipitation have led to a decrease in the Yellow River's natural runoff, and has consequently diminished sediment transport in the river channel, which has finally contributed to a persistent decline in terrestrial organic matter input since approximately 1970. From 1855 to 1949, cultivation and deforestation driven by rapid population growth have diminished forest cover, accelerated soil erosion, and consequently increased the terrestrial organic matter input during this period. Since around 1970, human activities such as dam construction, soil conservation measures, and increased water consumption have significantly reduced sediment discharge from the Yellow River. Notably, since the 1980s, the increased application of chemical fertilizers and discharge of wastewater have introduced substantial nutrient loads into estuarine and marginal sea areas, thereby maintaining an upward trend in total organic carbon and total nitrogen contents. It is noteworthy that after approximately 1970, although the mass accumulation rate showed a significant declining trend due to reduced sediment discharge, the organic carbon deposition rate exhibited a fluctuating but gradually increasing pattern, which may be largely attributed to enhanced marine productivity and elevated total organic carbon content. Consequently, the sedimentary record of the South Yellow Sea elucidates how climate variability and human activities modulate the carbon sink efficiency of a major marginal sea, providing a critical case for understanding carbon sequestration in land-ocean interaction zones under global change.

CRediT authorship contribution statement

Chuchu Zhang: Writing – original draft, Data curation, Conceptualization. **Yifei Qiu:** Software, Formal analysis. **Xiao Huang:** Methodology. **Xinqing Zou:** Writing – review & editing, Funding acquisition. **Min Xu:** Writing – review & editing, Funding acquisition. **Chenglong Wang:** Writing – review & editing, Funding acquisition.

Declaration of competing interest

The authors declare that they have no known competing financial interests or personal relationships that could have appeared to influence the work reported in this paper.

Acknowledgement

This study was supported by the Natural Science Foundation of China (Grant Nos. 42106056), the Fundamental Research Funds for the Central Universities (Grant Nos. 0209-14380134, 0209-14370407), the Natural Resources Science and Technology Project of Jiangsu Province (JSZRKJ202423).

Appendix A. Supplementary data

Supplementary data to this article can be found online at https://doi.org/10.1016/j.catena.2026.109963.

References

Aller, R.C., 2013. Sedimentary Diagenesis, Depositional Environments, and Benthic Fluxes: Treatise on Geochemistry.
Andersson, A., 2011. A systematic examination of a random sampling strategy for source apportionment calculations. Sci. Total Environ. 412-413, 232–238.
Berner, R.A., 1982. Burial of organic carbon and pyrite sulfur in the modern ocean; its geochemical and environmental significance. Am. J. Sci. 282 (4), 451–473.
Berner, R.A., 1990. Atmospheric carbon dioxide levels over phanerozoic time. Science 249 (4975), 1382–1386.
Bhushan, R., Dutta, K., Somayajulu, B.L.K., 2001. Concentrations and burial fluxes of organic and inorganic carbon on the eastern margins of the Arabian Sea. Mar. Geol. 178 (1–4), 95–113.
Bianchi, T.S., 2011. The role of terrestrially derived organic carbon in the coastal ocean: A changing paradigm and the priming effect. Proc. Natl. Acad. Sci. 108 (49), 19473–19481.
Blair, N.E., Aller, R.C., 2012. The fate of terrestrial organic carbon in the marine environment. Ann. Rev. Mar. Sci. 4 (1), 401–423.
Burdige, D.J., 2005. Burial of terrestrial organic matter in marine sediments: a re-assessment. Glob. Biogeochem. Cycles 19, GB4011.
Burdige, D.J., 2007. Preservation of organic matter in marine sediments: controls, mechanisms, and an imbalance in sediment organic carbon budgets? Chem. Rev. 107 (2), 467–485.
Cai, D., Sun, Y., Zhang, X., Su, Y., Wu, Y., Chen, Z., Yang, Q., 2014. Reconstructing a primary productivity history over the past 200a using sediment organic carbon content and the stable isotope composition from the East China Sea and the Yellow Sea. Acta Oceanol. Sin. 36 (2), 40–50.
Chen, J., Wang, F., Meybeck, M., He, D., Xia, X., Zhang, L., 2005. Spatial and temporal analysis of water chemistry records (1958–2000) in the Huanghe (Yellow River) basin. Glob. Biogeochem. Cycles 19 (3).
Chen, L., Liu, J., Xing, L., Krauss, K.W., Wang, J., Xu, G., Li, L., 2017. Historical changes in organic matter input to the muddy sediments along the Zhejiang-Fujian coast, China over the past 160 years. Org. Geochem. 111, 13–25.
Deng, J., Jin, X., 2000. Study on fishery biodiversity and its conservation in Laizhou Bay and Yellow River estuary. Zool. Res. 21 (1), 76–82.
Deng, B., Zhang, J., Wu, Y., 2006. Recent sediment accumulation and carbon burial in the East China Sea. Glob. Biogeochem. Cycles 20 (3).
Dittmar, T., Lara, R.J., 2001. Molecular evidence for lignin degradation in sulfate-reducing mangrove sediments (Amazônia, Brazil). Geochim. Cosmochim. Acta 65, 1417–1428.
Duan, S., Xing, L., Zhang, H., Feng, X., Yang, H., Zhao, M., 2014. Upwelling and anthropogenic forcing on phytoplankton productivity and community structure changes in the Zhejiang coastal area over the last 100 years. Acta Oceanol. Sin. 33 (10), 1–9.
Fan, H., Huang, H., 2008. Response of coastal marine eco-environment to river fluxes into the sea: A case study of the Huanghe (yellow) river mouth and adjacent waters. Mar. Environ. Res. 65 (5), 378–387.
Frangipane, A., Paris, E., 1994. Long-Term Variability of Sediment Transport in the Ombrone River Basin (Italy).
Fry, B., Sherr, E.B., 1984. δ13C measurements as indicators of carbon flow in marine and freshwater ecosystems. Contr. Mar. Sci. 27, 13–47.
Fuggle, R., Smith, W.T., Hydrosult Canada Inc., Agrodev Canada Inc., 2000. Large dams in water and energy resource development in the People's Republic of China (PRC). Country Review Paper Prepared as an Input to the World Commission on Dams, Cape Town. www.dams.org.
Gao, L.M., Yao, P., Wang, J.P., Zhao, B., 2016. Distribution and sources of organic carbon in surface sediments from the Bohai. Acta Oceanol. Sin. 38, 8–20.
Glazyrin, G.E., Tashmetov, H.K., 1995. Sediment Yield Alteration of Mountain Rivers and Climate Change in Central Asia.
Goldberg, E., Koide, M., 1963. Rates of Sediment Accumulation in the Indian Ocean.
Goñi, M.A., Hedges, J.I., 1995. Sources and reactivities of marine-derived organic matter in coastal sediments as determined by alkaline CuO oxidation. Geochim. Cosmochim. Acta 59 (14), 2965–2981.
Goñi, M.A., Ruttenberg, K.C., Eglinton, T.I., 1998. A reassessment of the sources and importance of land-derived organic matter in surface sediments from the Gulf of Mexico. Geochim. Cosmochim. Acta 62 (18), 3055–3075.
Gordon, E.S., Goñi, M.A., 2003. Sources and distribution of terrigenous organic matter delivered by the Atchafalaya River to sediments in the northern Gulf of Mexico. Geochim. Cosmochim. Acta 67 (13), 2359–2375.
Gordon, E.S., Goñi, M.A., Roberts, Q.N., Kineke, G.C., Allison, M.A., 2001. Organic matter distribution and accumulation on the inner Louisiana shelf west of the Atchafalaya River. Cont. Shelf Res. 21 (16–17), 1691–1721.
Guo, J., Yuan, H., Song, J., Li, X., Duan, L., Li, N., Wang, Y., 2021. Evaluation of sedimentary organic carbon reactivity and burial in the eastern China marginal seas. J. Geophys. Res. Oceans. 126 (4), e2021JC017207.
Hedges, J.I., Keil, R.G., 1995. Sedimentary organic matter preservation: an assessment and speculative synthesis. Mar. Chem. 49 (2–3), 137–139.
Hao, Z., Wang, J., L, L., Wang, Z., Wang, L., 2006. Impact of climate change on runoff in source region of Yellow River. J. Glaciol. Geocryol. 28 (1), 1–7.
Hedges, J.I., Blanchette, R.A., Weligy, K., Devol, A.H., 1988. Effects of fungal degradation on the CuO oxidation products of lignin: a controlled laboratory study. Geochim. Cosmochim. Acta 52, 2717–2726.
Hedges, J.I., Keil, R.G., Benner, R., 1997. What happens to terrestrial organic matter in the ocean? Org. Geochem. 27 (5–6), 195–212.
Houel, S., Louchouarn, P., Lucotte, M., Canuel, R., Ghaleb, B., 2006. Translocation of soil organic matter following reservoir impoundment in boreal systems: implications for in situ productivity. Limnol. Oceanogr. 51, 1497–1513.
Hu, L., Shi, X., Bai, Y., Qiao, S., Li, L., Yu, Y., Yang, G., Ma, D., Guo, Z., 2016. Recent organic carbon sequestration in the shelf sediments of the Bohai Sea and Yellow Sea, China. J. Mar. Syst. 155, 50–58.
Huang, M., Zhang, L., 2004. Hydrological responses to conservation practices in a catchment of the loess plateau, China. Hydrol. Process. 18 (10), 1885–1898.
Huang, Y., Freeman, K.H., Eglinton, T.I., 1999. $\delta^{13}C$ analyses of individual lignin phenols in quaternary lake sediments: A novel proxy for deciphering past terrestrial vegetation changes. Geology 27 (5), 471–474.
Huang, C.C., Pang, J., Su, H., Li, S., Ge, B., 2009. Holocene environmental change inferred from the loess–palaeosol sequences adjacent to the floodplain of the Yellow River, China. Quat. Sci. Rev. 28 (25–26), 2633–2646.
Kuzyk, Z.Z.A., Goñi, M.A., Stern, G.A., Macdonald, R.W., 2008. Sources, pathways and sinks of particulate organic matter in Hudson Bay: evidence from lignin distributions. Mar. Chem. 112 (3–4), 215–229.

Lamb, A.L., Wilson, G.P., Leng, M.J., 2006. A review of coastal palaeoclimate and relative sea-level reconstructions using δ13C and C/N ratios in organic material. Earth Sci. Rev. 75 (1–4), 29–57.
Li, F.Y., Gao, S., Jia, J.J., Zhao, Y.Y., 2002. Modern sedimentation rates in the muddy sedimentation areas of the Yellow Sea and Bohai Sea. Oceanologia et Limnologia Sinica 33 (4), 364–369.
Li, D., Yao, P., Bianchi, T.S., Zhang, T., Zhao, B., Pan, H., Wang, J., Yu, Z., 2014. Organic carbon cycling in sediments of the Changjiang estuary and adjacent shelf: implication for the influence of three gorges dam. J. Mar. Syst. 139, 409–419.
Li, D., Yao, P., Bianchi, T.S., Zhao, B., Pan, H., Zhang, T., Wang, J., Xu, B., Yu, Z., 2015a. Historical reconstruction of organic carbon inputs to the East China Sea inner shelf: implications for anthropogenic activities and regional climate variability. The Holocene 25, 1869–1881.
Li, J., Zheng, B., Hu, X., Wang, Y., Ding, Y., Liu, F., 2015b. Terrestrial input and nutrient change reflected by sediment records of the Changjiang River estuary in recent 80 years. Acta Oceanol. Sin. 37 (2), 27–35.
Liu, J.P., Xu, K.H., Li, A.C., Milliman, J.D., Velozzi, D.M., Xiao, S.B., Yang, Z.S., 2007. Flux and fate of Yangtze River sediment delivered to the East China Sea. Geomorphology 85 (3–4), 208–224.
Liu, L., Wei, G., Wang, J., Guan, Y., Wong, C.S., Wu, F., Zeng, E.Y., 2013. Anthropogenic activities have contributed moderately to increased inputs of organic materials in marginal seas off China. Environ. Sci. Technol. 47 (20), 11414–11422.
Liu, C., Wang, P., Wen, T., 2021. Spatio-temporal characteristics of climate change in the Yellow River source area from 1960 to 2019. Arid Zone Res. 38 (02), 293–302.
Lu, X., Higgitt, D.L., 1998. Recent changes of sediment yield in the upper Yangtze, China. Environ. Manage. 22 (5), 697–709.
Meade, R.H., Parker, R., 1985. Sediments in rivers of the United States. In: National Water Summary 1984, 2275. U.S. Geological Survey Water-Supply Paper, pp. 49–60.
Meyers, P.A., 1994. Preservation of elemental and isotopic source identification of sedimentary organic matter. Chem. Geol. 114 (3–4), 289–302.
Meyers, P.A., 1997. Organic geochemical proxies of paleoceanographic, paleolimnologic, and paleoclimatic processes. Org. Geochem. 27 (5–6), 213–250.
Milliman, J.D., Meade, R.H., 1983. World-wide delivery of river sediment to the oceans. J. Geol. 91, 1–21.
Moon, J.H., Hirose, N., Yoon, J.H., 2009. Comparison of wind and tidal contributions to seasonal circulation of the Yellow Sea. J. Geophys. Res. Oceans 114 (C8).
Nilsson, C., Reidy, C.A., Dynesius, M., Revenga, C., 2005. Fragmentation and flow regulation of the world's large river systems. Science 308 (5720), 405–408.
Park, Y.A., Khim, B.K., 1990. Clay minerals of the recent fine-grained sediment on the Korean continental shelves. Cont. Shelf Res. 10, 1179–1191.
Qiao, S.Q., Shi, X.F., Wang, G.Q., Zhou, X., Hu, B.Q., Hu, L.M., Yang, G., Liu, Y.G., Yao, Z. Q., Liu, S.F., 2017. Sediment accumulation and budget in the Bohai Sea, Yellow Sea and East China Sea. Mar. Geol. 390, 270–281.
Qu, B., Song, J., Yuan, H., 2018. Sediment records and responses for anthropogenic activities of organic matter in the Daya bay during recent one hundred years. Haiyang Xuebao 40 (10), 119–130.
Ren, M., Zhu, X., 1994. Anthropogenic influences on changes in the sediment load of the Yellow River, China, during the Holocene. The Holocene 4, 314–320.
Saito, Y., Yang, Z., Hori, K., 2001. The Huanghe (Yellow River) and Changjiang (Yangtze River) deltas: a review on their characteristics, evolution and sediment discharge during the Holocene. Geomorphology 41 (2–3), 219–231.
Shi, N., Yang, Y., 1998. Main characteristics of east Asian winter/summer monsoon index for 1873~1991. J. Nanjing Institute Meteorol. 02, 47–53.
Shi, X., Liu, S., Qiao, S., Liu, Y., Fang, X., Wu, Y., Zhu, Z., 2010. Depositional features and palaeoenvironmental records of the mud deposits in min-Zhe coastal mud area. Mar. Geol. Quat. Geol. 30 (04), 19–30.
Shi, X., Wu, B., Qiao, S., Yao, Z., Hu, L., Bai, Y., Hu, S., Sheng, J., Liu, Y., Liu, S., Wang, K., Zou, J., 2024. Distribution, burial fluxes and carbon sink effect of sedimentary organic carbon in the eastern China seas. Sci. China Earth Sci. 67 (10), 3062–3082.
Sikes, E.L., Uhle, M.E., Nodder, S.D., Howard, M.E., 2009. Sources of organic matter in a coastal marine environment: Evidence from n-alkanes and their $\delta^{13}C$ distributions in the Hauraki Gulf, New Zealand. Mar. Chem. 113 (3-4), 149–163.
Stanley, J.D., Warne, A.G., 1998. Nile delta in its destruction phase. J. Coast. Res. 14 (3), 794–825.
Sun, X., Fan, D., Liu, M., Liao, H., Tian, Y., 2020. The fate of organic carbon burial in the river-dominated East China Sea: evidence from sediment geochemical records of the last 70 years. Org. Geochem. 143, 103999.
Syvitski, J.P.M., Vörösmarty, C.J., Kettner, A.J., Green, P., 2005. Impact of humans on the flux of terrestrial sediment to the global Coastal Ocean. Science 308 (5720), 376–380.
Tang, Q., Jin, X., Wang, J., Zhuang, Z., Cui, Y., Meng, T., 2003. Decadal-scale variations of ecosystem productivity and control mechanisms in the Bohai Sea. Fish. Oceanogr. 12 (4–5), 223–233.
Tesi, T., Miserocchi, S., Goñi, M.A., Langone, L., 2007. Source, transport and fate of terrestrial organic carbon on the western Mediterranean Sea, gulf of lions, France. Mar. Chem. 105 (1–2), 101–117.
Tyson, R., 1995. Sedimentary Organic Matter: Organic Facies and Palynofacies.
Walling, D.E., Fang, D., 2003. Recent trends in the suspended sediment loads of the world's rivers. Glob. Planet. Change 39 (1–2), 111–126.
Wang, F., Chen, J., 2009. Asia-eastern Asia. In: Likens, G.E. (Ed.), Encyclopedia of Inland Waters. academic press, Oxford, pp. 306–317.
Wang, G., Han, J., Liu, D., 2003. The carbon isotope composition of C3 herbaceous plants in loess area of northern China. Sci. China Series D: Earth Sci. 46 (10), 1069–1076.
Wang, H., Yang, Z., Saito, Y., Liu, J.P., Sun, X., 2006a. Interannual and seasonal variation of the Huanghe (Yellow River) water discharge over the past 50 years: connections to impacts from ENSO events and dams. Glob. Planet. Change 50 (3–4), 212–225.
Wang, L., Shao, M.A., Wang, Q., Gale, W.J., 2006b. Historical changes in the environment of the Chinese loess plateau. Environ. Sci. Policy 9 (7–8), 675–684.
Wang, H., Yang, Z., Saito, Y., Liu, J.P., Sun, X., Wang, Y., 2007. Stepwise decreases of the Huanghe (Yellow River) sediment load (1950–2005): impacts of climate change and human activities. Glob. Planet. Change 57 (3–4), 331–354.
Wang, J., Yao, P., Bianchi, T.S., Li, D., Zhao, B., Cui, X., Pan, H., Zhang, T., Yu, Z., 2015. The effect of particle density on the sources, distribution, and degradation of sedimentary organic carbon in the Changjiang estuary and adjacent shelf. Chem. Geol. 402, 52–67.
Wang, S., Fu, B., Piao, S., Lü, Y., Ciais, P., Feng, X., Wang, Y., 2016. Reduced sediment transport in the Yellow River due to anthropogenic changes. Nat. Geosci. 9 (1), 38–41.
Wang, B., Xin, M., Wei, Q., Xie, L., 2018. A historical overview of coastal eutrophication in the China seas. Mar. Pollut. Bull. 136, 394–400.
Wang, C., Hao, Z., Gao, J., Feng, Z., Ding, Y., Zhang, C., Zou, X., 2020. Reservoir construction has reduced organic carbon deposition in the East China Sea by half since 2006. Geophys. Res. Lett. 47 (17).
Wang, H., Kandasamy, S., Liu, Q., Lin, B., Lou, J., Veeran, Y., Lei, H., Liu, Z., Arthur Chen, C., 2021. Roles of sediment supply, geochemical composition and monsoon on organic matter burial along the longitudinal mud belt in the East China Sea in modern times. Geochim. Cosmochim. Acta 305, 66–86.
Wang, S., Song, S., Zhang, H., Yu, L., Jiao, C., Li, C., Fu, B., 2025. Anthropogenic impacts on the Yellow River Basin. Nat. Rev. Earth Environ. 6, 656–671.
Winogradow, A., Pempkowiak, J., 2014. Organic carbon burial rates in the Baltic Sea sediments. Estuar. Coast. Shelf Sci. 138, 27–36.
Wu, X., Duan, H., Bi, N., Yuan, P., Wang, A., Wang, H., 2016. Interannual and seasonal variation of chlorophyll-a off the Yellow River mouth (1997–2012): dominance of river inputs and coastal dynamics. Estuar. Coast. Shelf Sci. 183, 402–412.
Wu, L., Fu, P., Xu, L., Wei, Y., Zhou, X., Li, Y., Wang, X., Zhou, Y., Liu, X., 2017. Changes in the source of sedimentary organic matter in the marginal sea sediments of eastern Hainan Island in response to human activities during the past 200 years. Quat. Int. 440, 150–159.
Wu, X., Wang, H., Bi, N., Saito, Y., Xu, J., Zhang, Y., Lu, T., Cong, S., Yang, Z., 2020. Climate and human battle for dominance over the Yellow River's sediment discharge: from the mid-Holocene to the Anthropocene. Mar. Geol. 425, 106188.
Xiao, R., Wu, X., Du, J., Deng, B., Xing, L., 2020. Impacts of anthropogenic forcing on source variability of sedimentary organic matter in the Yellow River estuary over the past 60 years. Mar. Pollut. Bull. 151, 110818.
Xing, L., Zhao, M., Zhang, H., 2009. Biomarker records of phytoplankton community structure changes in the Yellow Sea over the last 200 years. Period. Ocean Univ. China 39 (2), 317–322.
Xing, L., Zhang, H., Yuan, Z., Sun, Y., Zhao, M., 2011. Terrestrial and marine biomarker estimates of organic matter sources and distributions in surface sediments from the East China Sea shelf. Cont. Shelf Res. 31 (10), 1106–1115.
Xing, L., Hou, D., Wang, X., Li, L., Zhao, M., 2016. Assessment of the sources of sedimentary organic matter in the Bohai Sea and the northern Yellow Sea using biomarker proxies. Estuar. Coast. Shelf Sci. 176, 67–75.
Xu, J., 2003. Sediment flux to the sea as influenced by changing human activities and precipitation: example of the Yellow River, China. Environ. Manage. 31 (3), 328–341.
Xu, J., 2004. A study of anthropogenic seasonal rivers in China. Catena 55 (1), 17–32.
Xu, J., 2005. The water fluxes of the Yellow River to the sea in the past 50 years, in response to climate change and human activities. Environ. Manag. 35 (5), 620–631.
Xu, J., Zhu, Q., Zhou, T., 1999. Sudden and periodic changes ofEast Asian winter monsoon in the past century. Q. J. Appl. Meteorol. 10, 1–8.
Yang, Z., Milliman, J.D., Galler, J., Liu, J., Sun, X., 1998. Yellow River's water and sediment discharge decreasing steadily. EOS 79, 589–592.
Yang, Z., Wang, H., Saito, Y., Milliman, J.D., Xu, K., Qiao, S., Shi, G., 2006. Dam impacts on the Changjiang (Yangtze) river sediment discharge to the sea: the past 55 years and after the three gorges dam. Water Resour. Res. 42 (4).
Yang, Z., Ji, Y., Bi, N., Lei, K., Wang, H., 2011. Sediment transport off the Huanghe (Yellow River) delta and in the adjacent Bohai Sea in winter and seasonal comparison. Estuar. Coast. Shelf Sci. 93 (3), 173–181.
Yang, S., Yang, Q., Liu, S., Cai, D., Qu, K., Sun, Y., 2015. Burial fluxes and sources of organic carbon in sediments of the Central Yellow Sea mud area over the past 200 years. Acta Oceanol. Sin. 34 (10), 13–22.
Yu, H., Wu, Y., Zhang, J., Yao, Q.Z., Zhu, Z.Y., 2007. The characteristics of lignin of plants and soil samples in the Yangtze River (Changjiang) drainage basin. Acta Sci. Circumst. 27, 817–823.
Yu, H., Wu, Y., Zhang, J., Deng, B., Zhu, Z., 2011. Impact of extreme drought and the three gorges dam on transport of particulate terrestrial organic carbon in the Changjiang (Yangtze) river. J. Geophys. Res. 116 (F4).
Yuan, D., Zhu, J., Li, C., Hu, D., 2008. Cross-shelf circulation in the yellow and East China seas indicated by MODIS satellite observations. J. Mar. Syst. 70 (1–2), 134–149.
Zhang, L., 2005. The Study on Relationship between Characteristics of East Asian Winter/Summer Monsoon Intensity Indices and the Large Scale Southern/Northern Drought/Flood in China from 1951 to 2003. Nanjing University Of Information Science & Technology.
Zhang, T., 2012. Sedimentary Records of Lignin in Yellow Sea and East China Sea and the Application to the Study of Fate of Terrestrial Organic Carbon and Environmental Change. Ocean University of China.
Zhang, X., Wang, L., Si, F., 2001. Prediction of water consumption in the Huanghe river basin. Water Resources Hydropower Technol. 6, 8–13 (in Chinese).

Zhang, S., Jia, S., Liu, C., Cao, W., Hao, F., Liu, J., Yan, H., 2004. Hydrological cycle in the Huanghe source area and its influence. Sci. China (E series) 34 (Supp.I), 117–125.
Zhang, J., Wu, Y., Jennerjahn, T.C., Ittekkot, V., He, Q., 2007. Distribution of organic matter in the Changjiang (Yangtze River) estuary and their stable carbon and nitrogen isotopic ratios: implications for source discrimination and sedimentary dynamics. Mar. Chem. 106 (1–2), 111–126.
Zhang, L.J., Xu, X.M., He, H.J., 2009. POC content in size-fractioned TSS and transportation character in the Yellow River. Environ. Sci. 30 (02), 342–347.
Zhang, C., Qiu, Y., Dong, Z., Wang, C., Wang, Y., Liao, Q., Zou, X., 2024. Natural and anthropogenic forcing on the fate of sedimentary organic matter in the South Yellow Sea during the Holocene. Palaeogeogr. Palaeoclimatol. Palaeoecol. 634, 111958.
Zhao, B., Yao, P., Bianchi, T.S., Yu, Z.G., 2021. Controls on organic carbon burial in the eastern China marginal seas: a regional synthesis. Glob. Biogeochem. Cycles 35 (4).
Zhou, C., Dong, P., Li, G., 2015. Hydrodynamic processes and their impacts on the mud deposit in the southern Yellow Sea. Mar. Geol. 360, 1–16.
Zhu, X.J., Yu, G.R., Gao, Y.N., et al., 2012. Fluxes of particulate carbon from rivers to the ocean and their changing tendency in China. Prog. Geogr. 31 (01), 118–122.